RSC Advances

PAPER

View Article Online
View Journal | View Issue

Cite this: *RSC Adv.*, 2017, **7**, 55131

Visible-light-mediated antifungal bamboo based on Fe-doped TiO_2 thin films

Jingpeng Li, * Danjing Ren, Zaixing Wu, Chengjian Huang, Huimin Yang, Yuhe Chen and Hui Yu

TiO_2-based photocatalytic disinfection has been proved as one of the feasible approaches for the control and inhibition of the growth of mould fungi on woody materials. However, the wide band gap of TiO_2 (3.2 eV) limits the efficient absorption of sunlight in the visible region. In this study, visible-light-mediated antifungal bamboo based on Fe-doped TiO_2 thin films was successfully fabricated through a facile one-step homogeneous precipitation method. XRD studies confirmed that all of the as-prepared TiO_2 nanoparticles on the bamboo surface were anatase phase. Fe-doped TiO_2 thin films were found to grow on the bamboo surface by the self-aggregation of nanoparticles with an average diameter of about 9.7 nm and a surface area of about 90.96 $m^2\ g^{-1}$. The Fe-doped TiO_2/bamboo samples looked identical to original bamboo as there was no essential effect on the optical properties of the bamboo surface. Moreover, the antifungal activity of the as-prepared samples against mould fungi was investigated under natural weather conditions. Compared with original bamboo and TiO_2/bamboo, the Fe-doped TiO_2/bamboo exhibited much higher inhibition ability to mould fungi under the natural environment, which is due to the fact of the red shift of the absorption edge of the Fe-doped TiO_2 nanostructures on the bamboo surface. UV-vis DRS also revealed that the band gap of Fe-doped TiO_2 nanostructures was obviously decreased, extending the light response of TiO_2 from ultraviolet to the visible light region. The research result may provide a general and effective approach to prepare visible-light-driven photocatalysts used for inhibition of the growth of mould fungi on the surface of bamboo.

Received 11th September 2017
Accepted 23rd November 2017

DOI: 10.1039/c7ra10103a

rsc.li/rsc-advances

1. Introduction

Titanium dioxide (TiO_2) has been widely applied in various fields such as photocatalytic systems, antimicrobial materials, self-cleaning coatings, hydrogen production, and solar cells due to its remarkable chemical and physical properties.[1–5] Over the past several years, TiO_2 as an important semiconductor material and photocatalyst has received a lot of attention because of its biological and chemical inertness, nontoxicity, relatively low cost, long-term stability, and high photocatalytic efficiency. The US Food and Drug Administration (FDA) also approved its use in human foods, drugs, cosmetics, and use in the food industry, as a nontoxic material.[6] Since the early research of Matsunaga *et al.*[7] reported the first application of pure TiO_2 for the photocatalytic disinfection of microorganisms, research work on TiO_2-based photocatalysts for various microorganism disinfections, including viruses,[8] bacteria,[9] fungi,[10] algae,[11] and protozoa[12] has been carried out. It is widely considered that photocatalytic microorganism disinfection depends on the interaction between microorganisms and reactive oxygen species (ROS) generated from photocatalysts under light illumination, such as $^{\cdot}OH$ and $^{\cdot}O_2^-$, which can kill the microorganisms.[13] At present, this capability is very desirable for the inhibition to the growth of mould fungi on bamboo surface. Bamboo as a rapidly renewable sustainable resource, can be available for building, flooring, roofing, fabrics and cloth, pulp and paper, and charcoal. The traditional markets for bamboo products were dominated by the handicrafts, chopsticks, bamboo blinds, and daily necessities. With the development of modern processing techniques, bamboo can be transformed into many new products such as laminated furniture, flooring, and decoration constructions that can compete directly with wood products either in quality or in price.[14] However, bamboo is more susceptible to mould growth than wood, which allow them to adapt a wide range of humidity and temperature.[15] As known, TiO_2 is only active under UV light irradiation because of their wide band gap energy (3.2 eV), which only about 5% of solar light can be utilized. Thus, it is high time to develop novel TiO_2-based photocatalysts that can yield high photocatalytic activity under visible light illumination so that a greater portion of the solar spectrum could be utilized.

Numerous efforts have been carried out in the past decades to develop the visible-light-driven TiO_2-based photocatalysts by impurity doping, metallization, sensitization and coating, *etc.*[16,17] Among these techniques, metal ion doped TiO_2 has been

China National Bamboo Research Center, Key Laboratory of High Efficient Processing of Bamboo of Zhejiang Province, Hangzhou 310012, PR China. E-mail: lijp@caf.ac.cn

extensively studied due to not only the expanded spectral response but also the improved photocatalytic activity.[18–20] Choi *et al.*[21] demonstrated that metal ions (Fe^{3+}, Ag^{+}, Co^{2+}, V^{3+}, Rb^{+}, Ni^{2+}, Cu^{2+}, Ru^{3+}, *etc.*) doping results in a red-shift of the photophysical response of TiO_2. Among various dopants, Fe^{3+} is the suitable candidate because of their band-gap (~2.6 eV) and similar size to that of Ti^{4+}, and Fe^{3+}-doped nanostructured TiO_2 also showed an antibacterial behavior.[22] Its unique half-filled electronic configuration, which might narrow the energy gap through the formation of new intermediate energy levels and also diminish recombination of electrons and holes by capturing photogenerated carriers.[23] Up to now, Fe^{3+} doped nanostructured TiO_2 has rarely been used for photocatalytic disinfection of specific microorganisms, let alone use for disinfection the mould fungi of bamboo surface. Meanwhile, the antimicrobial activities of Fe-doped TiO_2 thin films have been studied by a few groups of researchers.[24–27] However, due to its much larger size and thicker cell wall/membrane, the mould fungi usually have stronger resistance to ROS attack than bacteria or viruses. Thus, effective alternatives to chemical fungicides are difficult to develop. Because of the demonstrated strong photocatalytic disinfection effect under visible light illumination and environmental friendliness of Fe-doped nanostructured TiO_2, they might provide an efficient fungicidal agent for the inhibition to the growth of mould fungi on woody materials.

To the best of our knowledge, it has been found that no reported studies are available on the application of Fe-doped TiO_2 nanoparticles to inhibit fungal growth on the surface of bamboo in the presence of solar light. Herein, we present a facile method to anchor the Fe-doped TiO_2 thin films on the surface of bamboo. The effect of Fe^{3+} dopants on the morphology, structure, composition, surface area, and band gap of TiO_2 nanoparticles on the surface of bamboo was also investigated. The visible-light-mediated photocatalytic inhibition of mould fungi using the Fe-doped TiO_2 nanoparticles has been verified in the absence and presence of solar light.

2. Experimental

2.1. Materials

All the chemical agents were analytical grade and used without further purification. Deionized (DI) water was used in the entire experiment. Moso bamboo specimens with the sizes of 50 mm × 20 mm × 6 mm were ultrasonically cleaned in DI water for 30 min, and then dried at 60 °C for 24 h.

2.2. Synthesis of Fe-doped TiO_2 thin films on bamboo surface

Ammonium fluotitanate ($(NH_4)_2TiF_6$) was used as the titanium source. Urea ($CO(NH_2)_2$) which releases ammonia *via* forced hydrolysis in DI water, was used to control the precipitation reaction. Iron nitrate nonahydrate ($Fe(NO_3)_3 \cdot 9H_2O$) was used as a source for Fe^{3+} doping. In a typical synthesis process, $(NH_4)_2TiF_6$ (1.5 g), $CO(NH_2)_2$ (15.0 g) and $Fe(NO_3)_3 \cdot 9H_2O$ (0.0606 g) were dissolved in 500 mL of DI water under vigorous magnetic stirring. The n_{Fe}/n_{Ti} molar ratio is 2.0 at%. After stirring for 5 min at room temperature (RT), bamboo samples were subsequently placed into the reaction solution. The final solution was heated to 90 °C under magnetic stirring for 2 h. After cooling naturally to RT, the bamboo specimens were taken out and cleaned in DI water by an ultrasonic bath for 3 min. The resultant particles in reaction solution were recovered *via* centrifugation, and washed repeatedly with DI water. At last, all the samples were dried at 80 °C for 24 h. The pure TiO_2 nanoparticles were prepared on the surface of bamboo with the same procedure described above but without the addition of $Fe(NO_3)_3 \cdot 9H_2O$. In this paper, the undoped TiO_2/bamboo was labeled as TiO_2B. The Fe-doped TiO_2/bamboo was labeled as $FeTiO_2$B and pure Fe-doped TiO_2 particle was labeled as $FeTiO_2$.

2.3. Characterization

The X-ray diffraction (XRD) analysis was performed on a Rigaku D/Max 2500 X-ray diffractometer with Cu Kα radiation (λ = 1.5418 Å) at a generator voltage of 40 kV and a generator current of 30 mA with a scanning speed of 4° min^{-1} from 10° to 90°. The compositions of the products were inferred from the X-ray photoelectron spectroscopy (XPS, PHI Quantera XPS) on a PHI-5000C ESCA system with Al Kα X-rays as the excitation source. The surface morphologies of the samples were observed by scanning electron microscopy (SEM, JEOL JSM-7610F, Japan). Specific surface areas of the as-prepared samples were measured based on the linear portion of the Brunauer–Emmett–Teller (BET, Quantachrome of Micromeritics ASAP 2020 instruments, USA). The UV-vis absorption spectra of the samples were recorded using a UV-vis spectrophotometer (UV-vis, Hitachi U-3900, Japan).

2.4. Mould resistance test

The field test was performed in Hangzhou city, China (N 30°17′25″, E 120°6′53″, 10 m above sea level). In order to keep the same environment, all specimens were placed horizontally, 1.2 m above the ground, in an outdoor test field fully exposed to sun, rain and wind (Fig. 1a). The bamboo samples were exposed outdoors from Jun 4th to Jul 3rd (2017), which are easily to mould in the rainy season. Temperature, relative humidity, and precipitation at the test site were recorded as shown in Fig. 1b–d. It is noteworthy that there is no sunny day in this period of time and the ultraviolet index is quite low at daytime. The control group was carried out in the same condition without natural light. The mould coverage on bamboo substrate was evaluated according to EN 927-3 (2000).[28]

3. Results and discussion

Mildew is an urgent problem in the bamboo processing industry. Especially in outdoor applications, bamboo is very easy to mould in the rainy season. The effective fungicidal methods used for bamboo rely heavily on synthetic chemical pesticide, such as sodium pentachlorophenate.[29] However, it is usually hazardous to animals, humans, and the environment. Furthermore, mould fungi have developed resistance to some

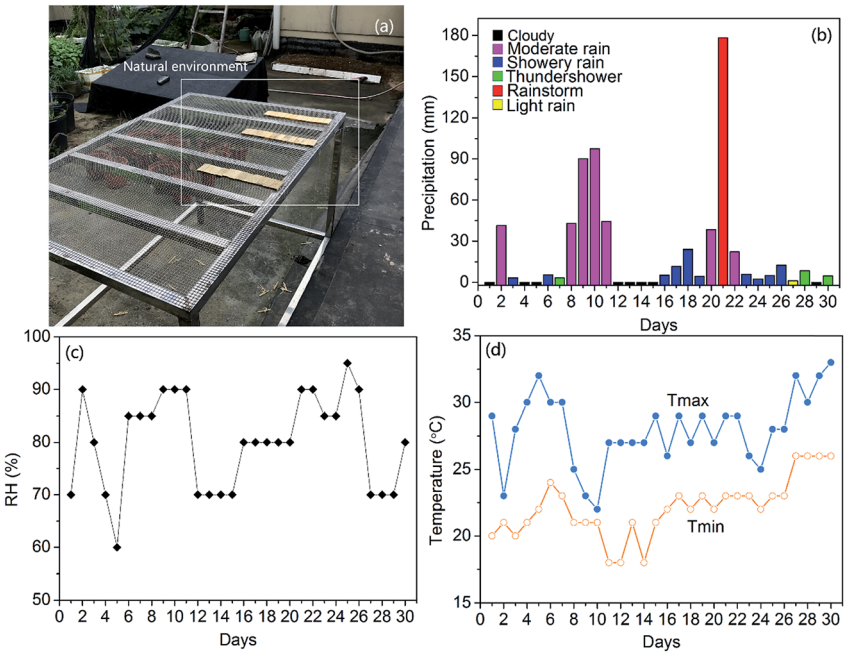

Fig. 1 (a) Field test. (b) Precipitation, (c) relative humidity, and (d) temperature at the test site from Jun 4th until Jul 3rd.

current fungicides, which is always hard to inhibit fungal growth of bamboo. Thus, alternative antifungal techniques used for bamboo need to be developed, which should overcome the fungicide resistance for a better fungicidal effect. Since the photocatalytic disinfection of microorganism using TiO_2 was first successful reported by Matsunaga *et al.*[7] Considerable studies have been conducted on TiO_2-based photocatalysts for various microorganism disinfections. However, the large band gap of TiO_2 and low quantum efficiency restrict its wide application. Thus, it is high time to develop novel photocatalysts that can yield high photocatalytic activity under visible light so that a greater portion of the solar spectrum could be utilized. As depicted in Fig. 2, the Fe-doped TiO_2 nanoparticles were successfully fabricated on the surface of bamboo. By doping the Fe ions in TiO_2 matrix results in significantly extending for its optical responses from UV to visible region. The resulted Fe-doped TiO_2/bamboo samples exhibit powerful ability to against mould fungi under natural environment than the original bamboo and TiO_2/bamboo, which will be demonstrated by fungi inhibition tests in subsequent paragraphs.

3.1. Phase structures

XRD spectra of the as-prepared pure TiO_2 nanoparticles and $FeTiO_2$ nanoparticles were presented in Fig. 3. It is observed that the diffraction peaks of two samples are ascribed to the

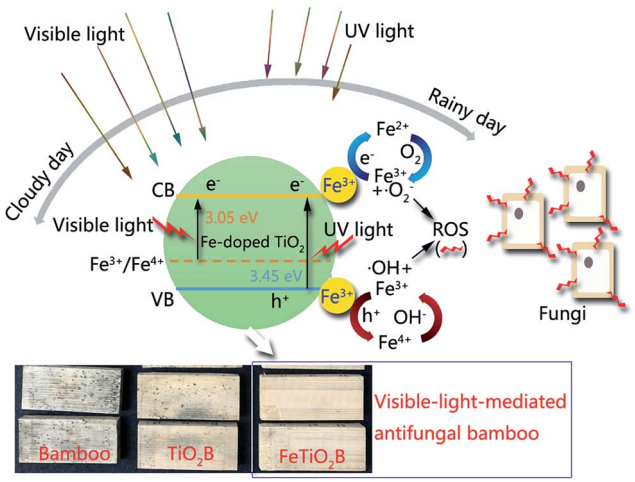

Fig. 2 Bamboo decorated with Fe-doped TiO_2 thin films for fungi inhibition.

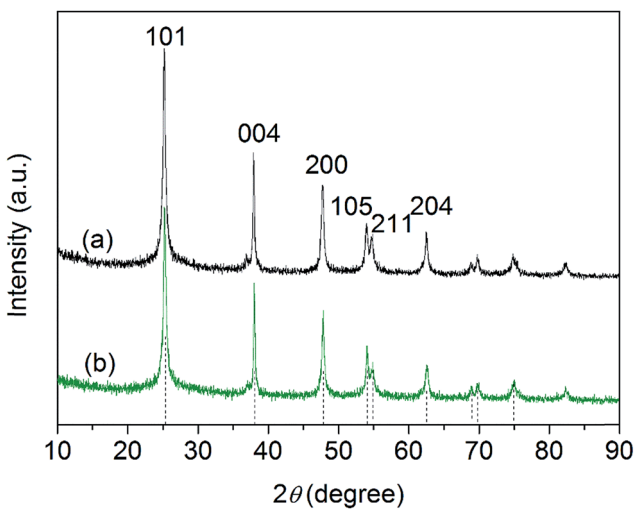

Fig. 3 XRD patterns of (a) pure TiO_2 and (b) $FeTiO_2$ nanoparticles.

peaks of anatase TiO_2 phase (JCPDS card no. 71-1167). It should be noted that no Fe_2O_3 or Fe_xTiO_y peak could be found in the XRD spectra. This result indicates that there has been virtually no phase change in TiO_2 during the doping process. The crystal sizes of TiO_2 nanoparticles and $FeTiO_2$ nanoparticles were estimated using the Scherrer equation:[30]

$$D = \frac{K\lambda}{\beta \cos \theta} \quad (1)$$

where β is the half-height width of the diffraction peak of anatase, $K = 0.89$ is a coefficient, θ is the diffraction angle, and λ is the X-ray wavelength corresponding to the Cu-Kα irradiation (λ = 1.5406 Å). By using the Scherrer equation, the crystallite sizes of TiO_2 and $FeTiO_2$ are calculated to be 12.5 and 9.7 nm, respectively. The average crystallite size of $FeTiO_2$ products is lower than that of pure TiO_2, which indicates the occurrence of a slight lattice distortion in the TiO_2 structure. The dimension decrease in crystallite size may be caused by a number of defects in the anatase crystallites produced by the substitution of part of the Ti(IV) site by Fe(III) cations.[31] In addition, the spacing between the (101) plane fringes of both samples was measured to be approximately 0.35 nm. No distinct spacing change was observed in $FeTiO_2$, suggesting that Fe was incorporated into the anatase crystal structure without changing the average dimension of the unit cell.[32]

3.2. XPS analysis

In order to investigate the chemical composition of Fe-doped TiO_2 on the surface of bamboo and determine the chemical status of Fe elements in the doped products, the as-prepared samples were measured by XPS. Fig. 4a presents the XPS survey spectra of the pristine bamboo, TiO_2B, and $FeTiO_2B$. It can be observed that the original bamboo contains C, O, and N elements. After decorating with pure TiO_2 nanoparticles, two new peaks of Ti and F elements were appeared on the surface of bamboo. It should be noted that the doped TiO_2 sample not only contains Ti, F, C, N and O elements, but also a small amount of Fe elements, which come from the Fe doping process. The C element can be ascribed to the bamboo substrate or the adventitious carbon based contaminant.

The high-resolution XPS spectra of the Ti 2p of TiO_2B and $FeTiO_2B$ samples are presented in Fig. 4b. The binding energy difference of 5.7 eV for the Ti $2p_{3/2}$ peak and Ti $2p_{1/2}$ peak of both products revealed a valence state of +4 for Ti, indicating that Ti was mostly Ti^{4+}. It should be noted that Ti 2p peak at 458.7 eV of $FeTiO_2B$ shifted positively by 0.1 eV in comparison with that of the Ti 2p peak in TiO_2B sample (458.8 eV). The shift of E_b could be ascribed to the interaction between host ion Ti^{4+} and foreign Fe-ions and the formation of the Ti–O–Fe bond in $FeTiO_2B$ sample. Fig. 4c displays the XPS spectra of N 1s for original bamboo and $FeTiO_2B$. We can see that the peak at approximately 398.5 eV was assigned to the nitrogen in C–N or O–N in original bamboo substrate. For $FeTiO_2B$ sample, a N 1s peak of weak intensity is observed at about 400.3 eV, which can be assigned to the surface adsorbed ammonium ions.[33] To investigate whether F atoms were incorporated in the titania lattice or not, the high-resolutions XPS spectrum of F 1s for $FeTiO_2B$ sample was recorded in Fig. 4d. Only one peak was detected in $FeTiO_2B$ sample. The peak at 682.8 eV is due to the adsorbed F^- ions on the surface of TiO_2. The large amount of surficial F^- ions may occur not only by electrostatic adsorption but also by nucleophilic substitution reaction of F^- ions and surficial hydroxyl groups.[34] The high-resolution XPS spectrum of the Fe 2p is presented in Fig. 4e. The peaks of Fe $2p_{3/2}$ and Fe $2p_{1/2}$ shown in Fig. 4e are located at 710.8 and 723.1 eV, respectively, corresponding well to the binding energy of Fe^{3+}.

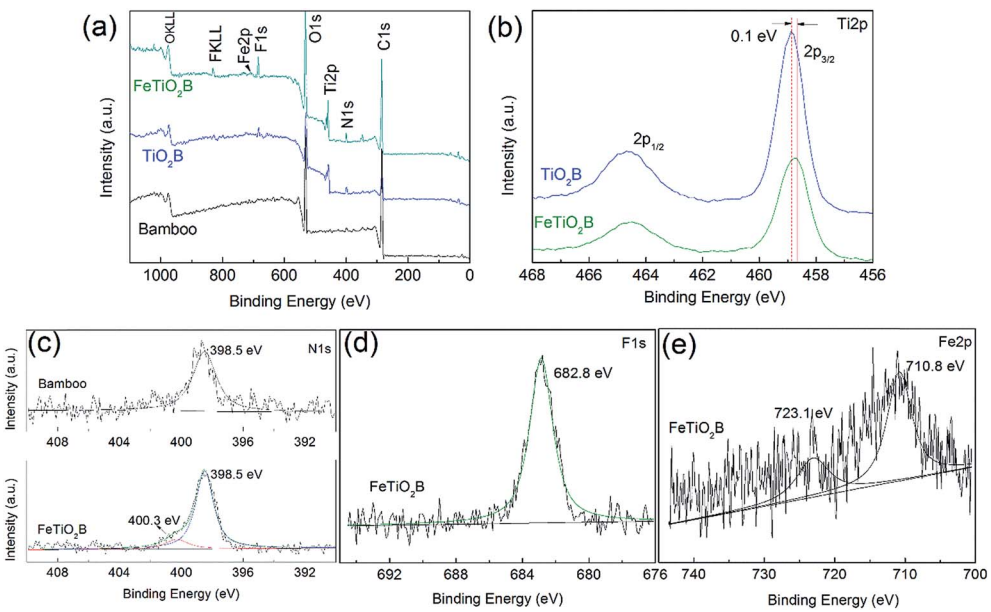

Fig. 4 (a) XPS survey spectra of the original bamboo, TiO_2B, and $FeTiO_2B$; high-resolution XPS spectra of (b) Ti 2p region of TiO_2B and $FeTiO_2B$, (c) N 1s region of original bamboo and $FeTiO_2B$, and (d) F 1s and (e) Fe 2p region of $FeTiO_2B$, respectively.

The low intensity of the Fe 2p peaks suggests that the incorporated Fe^{3+} ions do not accumulate at the nanoparticles surface layers but uniformly distribute in the titania matrix.

3.3. Morphological structures

The SEM images of the original bamboo, TiO_2B, and $FeTiO_2B$ are shown in Fig. 5. As shown in Fig. 5a, a typical SEM image of original bamboo surface, on which the microstructure of a longitudinal section of original bamboo whose vascular bundles were embedded in the matrix of ground parenchyma. A corresponding EDS spectrum for original bamboo was presented in Fig. 5a (inset). Only C, O, and Au elements could be detected from the spectra of the original bamboo. Au element originated from the coating layer used during the SEM observation, whereas C and O elements were from the bamboo. For TiO_2B sample (Fig. 5b), numerous TiO_2 nanoparticles can be observed on the surface of bamboo after precipitation process. This illustrates TiO_2 nanoparticles were successfully attached on the surface of bamboo *via* the facile one-step homogeneous precipitation method. In the corresponding EDS spectrum of the inset in Fig. 5b, three new signals from N, F, and Ti were detected in the spectrum of the TiO_2B sample. The N and F elements may be originated from the precursor $(NH_4)_2TiF_6$, and no other elements were detected, implying that the thin films were primarily TiO_2. Fig. 5c shows the SEM image of $FeTiO_2B$ at low magnification. More small nanoparticles are well-dispersed on bamboo surface. The bamboo surface is covered by a dense and even hierarchical film of $FeTiO_2$ nanoparticles. From the corresponding high-magnification SEM image in Fig. 5d, the nanoparticles with the sizes ranging from 20 to 100 nm are clearly visible. However, by using the Scherrer equation (Table 1), the average crystallite sizes of $FeTiO_2$ are calculated to be about 9.7 nm. Obviously, these nanoparticles were aggregated into larger particles on the surface of bamboo. As shown in Fig. 5d (inset), a signal from Fe was present in the spectrum of $FeTiO_2B$ sample after Fe doping, which further confirmed that the bamboo substrate was successfully modified by Fe-doped TiO_2. Furthermore, the Fe-doped TiO_2/bamboo sample looks identical to the original bamboo as there is no essential effect on the optical properties of the bamboo surface (Fig. 5, insets).

3.4. BET surface areas and pore distributions

The specific surface area of the as-prepared samples is measured using the BET method by N_2 adsorption and desorption at 77 K. Fig. 6 displays the N_2 adsorption–desorption isotherms of TiO_2 and $FeTiO_2$ products. Their pore size distributions are presented in the inset of Fig. 6. Both samples present a type-IV isotherm with an H_3 type hysteresis loop with distinct hysteresis loops observed in the relative pressure range of 0.6–1.0, which indicated that the nanoparticles were mesoporous materials. The BET surface area of the $FeTiO_2$ nanoparticles is calculated to be 90.96 $m^2\ g^{-1}$. Moreover, the pore diameter distribution of the $FeTiO_2$ indicates that the average pore diameter is about 11.20 nm. Furthermore, the pure TiO_2 sample has similar isotherm and pore diameter distribution and BET surface area, which is listed in Table 1. The formation of nanoporous structure in the products may be attributed to the aggregation of TiO_2 nanoparticles. Such nanoporous structures and large BET surface areas were crucial for photocatalysts, since they could supply transport channels for the molecules involved in the reaction and effectively separate photo-excited electron–hole pairs, reducing the recombination of electron–hole pairs.[35]

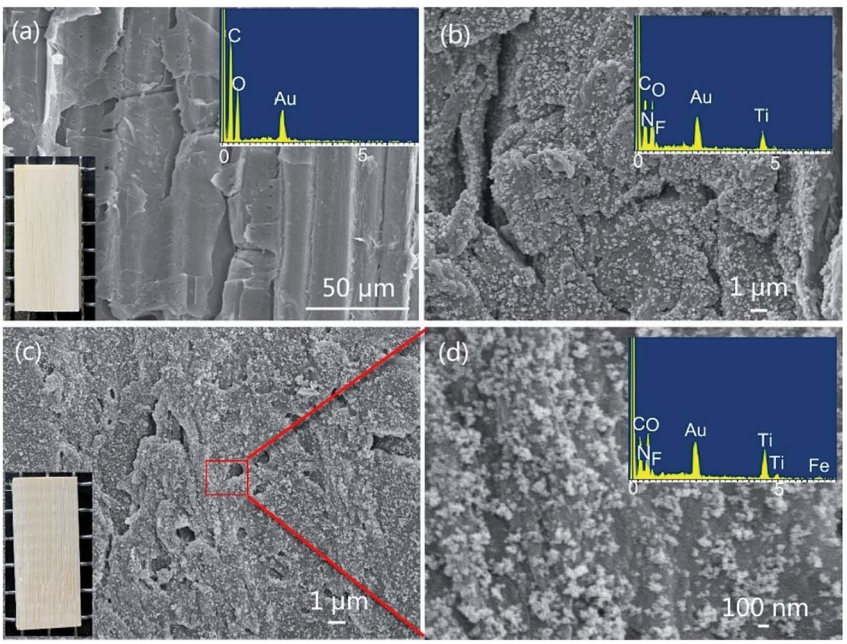

Fig. 5 SEM images of the (a) original bamboo, (b) TiO_2B, (c, d) $FeTiO_2B$ at different magnifications. The inset is the corresponding physical image and EDS spectra of bamboo samples.

Table 1 Physicochemical properties of the samples

Samples	Crystallite size (nm)	Plane fringes (101) (nm)	BET surface area ($m^2\ g^{-1}$)	Average pore size (nm)	Pore volume ($m^3\ g^{-1}$)	Band gap (eV)
TiO_2	12.5	0.35	73.64	11.99	0.217	3.20
$FeTiO_2$	9.7	0.35	90.96	11.20	0.237	3.05

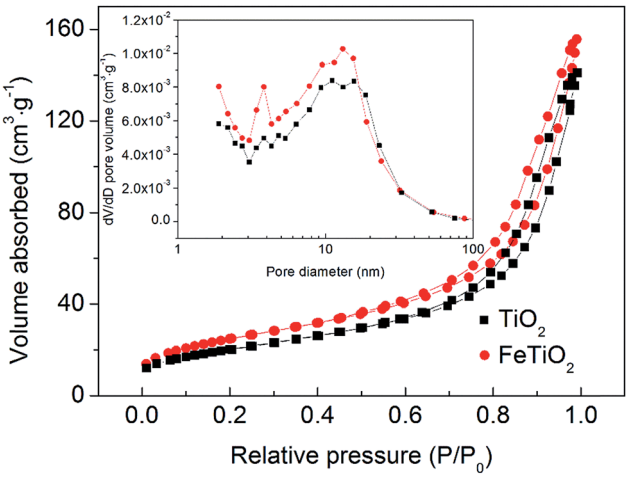

Fig. 6 N_2 adsorption–desorption isotherms and corresponding pore diameter distribution curves of the TiO_2 and $FeTiO_2$ samples.

3.5. UV-vis spectroscopy

UV-vis diffuse reflectance spectra of the pure TiO_2 and $FeTiO_2$ products were shown in Fig. 7. As shown in Fig. 7a, the pure TiO_2 nanoparticles only exhibit adsorption in UV-light region. Obviously, the diffuse reflectance spectra of $FeTiO_2$ presents a red shift and increases absorption in the visible-light range when Fe was doped into TiO_2 lattice. Compared with the pure TiO_2, these $FeTiO_2$ products exhibit absorption in both UV and visible-light regions. The direct band gap energy can be estimated from a plot of $(\alpha h\nu)^2$ *versus* photon energy ($h\nu$).[20] The absorption coefficient α and direct band gap E_g are related through the Kubelka–Munk function equation:[36,37]

$$(\alpha h\nu)^2 \propto h\nu - E_g \quad (2)$$

where ν is the frequency and h is Plank's constant. The band gap energies of the TiO_2 and $FeTiO_2$ products are shown in Table 1. The band gap energy of $FeTiO_2$ is 3.05 eV, which is lower than that of pure TiO_2 prepared by the same method (3.20 eV). The results indicated Fe doping can decrease the band gap energy of TiO_2, extending the utilization of the visible light. This is due to the fact that the doping Fe ions could create a donor level above the original valence band of TiO_2 to narrow the TiO_2 band gap.[38] This narrow band gap facilitated excitation of electrons from valence band to conduction band in $FeTiO_2$ under visible light, resulting in enhanced photoactivity.

3.6. Antifungal activity

Bamboo products without protection are very easy deteriorated by the complex interplay of microorganism and environment when exposed to the weather. Previous studies have shown that bamboo can allow mould fungi to adapt and survive over a wide range of humidity (63%~) and temperature (5–30 °C).[15] When the temperature and humidity were appropriate, spores of mould fungi on bamboo surface germinated and grew rapidly. As shown in Fig. 1, we can see that the humidity and temperature are suitable for growing mould fungi on the surface of bamboo in Hangzhou, especially in the rainy seasons. As expected, all model fungi grew differently according to the infected bamboo samples (Fig. 8). The biological colonization percentages by mould fungi on different bamboo samples are presented in Fig. 9. After two weeks, the original bamboo displayed poor resistance to mould fungi exposure and became rapidly covered with mould fungi (Fig. 8a). The mould fungi had created abundant mycelia on the sample surface and showed a fast propagation reaching a level of colonization of around 100%. In a similar manner, the mould fungi also attacked the TiO_2B samples, but colonization evolves in a slower manner than the original bamboo (final degree of colonization round 75% for TiO_2B samples). This is due to the

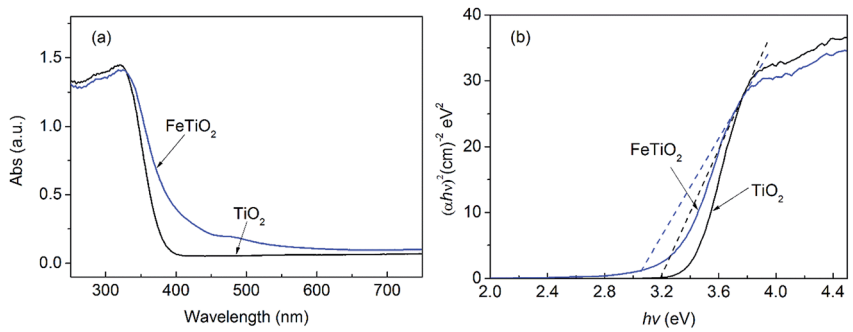

Fig. 7 (a) UV-vis diffuse reflectance spectra and (b) plots of $(\alpha h\nu)^2$ *vs.* $h\nu$ of the as-prepared samples.

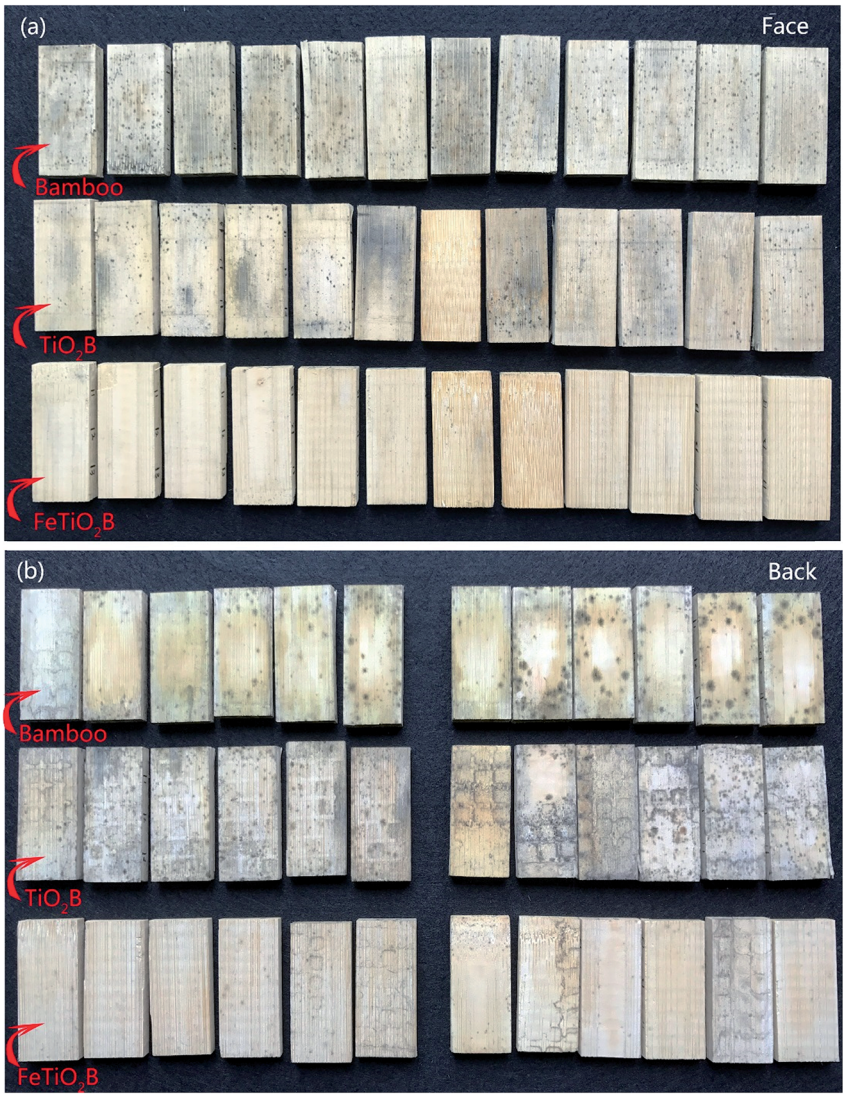

Fig. 8 Digital photograph of the as-prepared samples after two weeks exposure to the outdoor test field. (a) Face to the sun; (b) back to the sun.

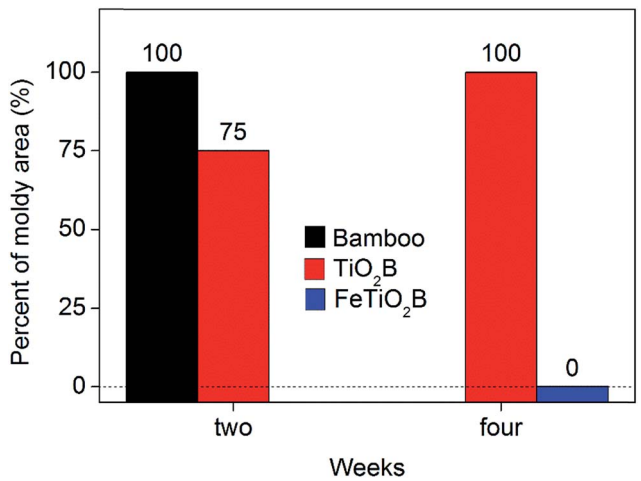

Fig. 9 Antifungal activity of the as-prepared samples after one-month exposure.

fact that in the presence of TiO_2 and UV light (solar light), ROS (such as hydroxyl radicals and superoxide radical anions) generated on the surface is considered responsible for the inactivation of the mould fungi. By contrast, the $FeTiO_2B$ samples showed efficiently resistance to mould growth. There is no mould fungi grown on the surface of bamboo (Fig. 8a). After one-month exposure under natural environment, we also saw no visible growth of $FeTiO_2B$ surface. The area of mould infection of $FeTiO_2B$ samples was zero (Fig. 9). However, we found that the area of mould infection of TiO_2B sample was reached 100% at the end of a month (Fig. 9). Furthermore, the photographs of the bottom surfaces of bamboo samples after two weeks exposure to the outdoor test field are shown in Fig. 8b. We can see that the original bamboo and TiO_2B samples were both infected by the mould fungi. Compared with the upper surfaces of TiO_2B samples, there are more mould fungi covered on the bottom surfaces of TiO_2B samples. The area of mould infection was reached 100% after two weeks. Our previous study have illuminated that TiO_2-coated film on bamboo surface in the presence of

solar light exhibited weak antifungal capability.[39] Though the weather in the test period was cloudy or rainy, a small amount of ultraviolet light could still shine on the surface of bamboo through the clouds. Therefore, the surface of TiO_2B sample, which is exposed to solar light, exhibits little higher antifungal activity than the shady face of sample. In contrast, $FeTiO_2B$ is different from the original bamboo and TiO_2B, the bottom surfaces of $FeTiO_2B$ still displayed an excellent antifungal activity without UV light (solar light) (Fig. 8b). The similar experimental results were presented in Fig. 10. The end face and side face of $FeTiO_2B$ both remained the high photocatalytic disinfection efficiency of mould fungi than the original bamboo and TiO_2B even under the natural environment. This high efficiency of mould fungi disinfection by the Fe-doped TiO_2 thin films was a result of the Fe doping, lead to the significantly extending of the optical responses from UV to visible region.

Based on the above investigation of the experimental parameters for TiO_2B and $FeTiO_2B$, we concluded that Fe doping can decrease the band gap energy of TiO_2, extending the utilization of the visible light. As shown in Fig. 2, even without UV light, the Fe-doped TiO_2 still presented higher visible light photocatalytic activity than that of pure TiO_2. Fe in $FeTiO_2B$ acted as an intermediate agent for the transfer of photo-generated electrons from the valence band to the conduction band of TiO_2. Therefore, Fe could contribute to the electron–hole pair separation efficiency and to inhibiting recombination

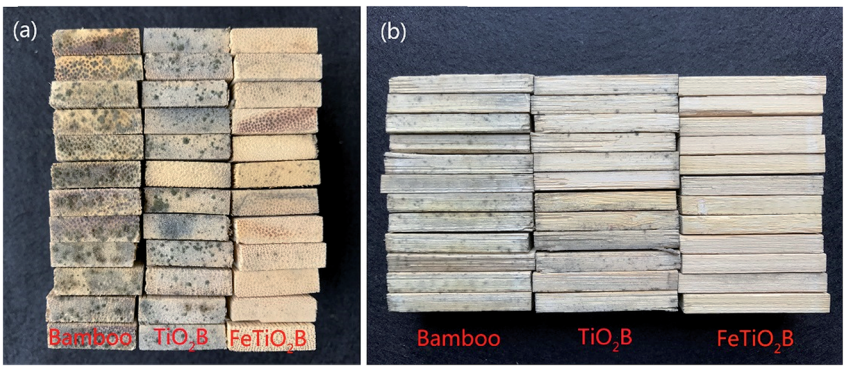

Fig. 10 Digital photograph of the as-prepared samples after two weeks exposure to the outdoor test field. (a) End face; (b) side face.

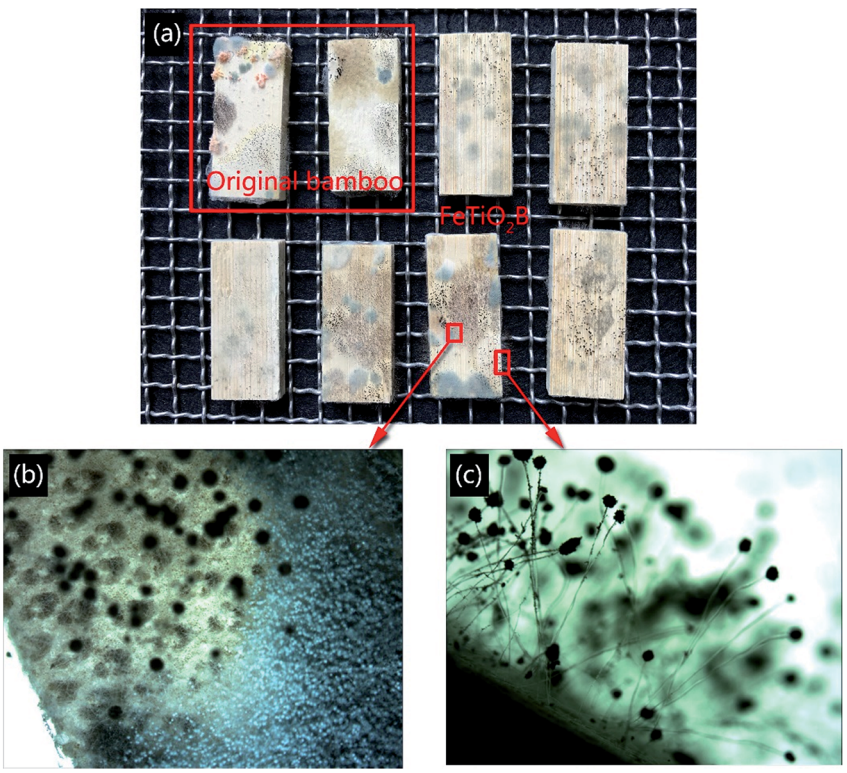

Fig. 11 (a) Digital photograph of original bamboo and $FeTiO_2B$ after one-week exposure in dark environments. (b, c) Optical microscope pictures of $FeTiO_2B$ sample colonized by mould fungi.

of the electrons and holes, leading to an increasing lifetime of generated electrons. According to the XPS results, Fe defected into the TiO_2 lattice produced Ti^{3+} ions could increase the electron–hole separation capacity of the photocatalyst, which is due to the production of oxygen vacancy (eqn (3)). Additionally, Fe^{3+} ions came into react with Ti^{3+} ions (eqn (4)) to promote the proceed of eqn (3) and produce more oxygen vacancy. That is, the presence of oxygen vacancy could reduce the band gap of TiO_2, and thus the electron–hole pairs could be easily generated when $FeTiO_2B$ was irradiated by even visible light. The photo-induced electron–hole pairs then reacted with water and molecular oxygen absorbed on the photocatalyst surface, and produced hydroxyl radicals ($^{\bullet}OH$) and superoxide radical anions ($^{\bullet}O_2^-$) (eqn (5)–(7)).[13,40] Moreover, Fe^{3+} ions would also react with the oxygen species and hydroxyl species adsorbed on the surfaces to form hydroxyl radicals ($^{\bullet}OH$) and superoxide radical anions ($^{\bullet}O_2^-$) (eqn (8)–(10)). Finally, these oxygen radicals attacked organic components of mould fungi resulting in its death (eqn (11)).[41]

$$TiO_2 + O_2^- \rightarrow 2Ti^{4+} + 2Ti^{3+} + 0.5O_2 \quad (3)$$

$$Fe^{3+} + Ti^{3+} \rightarrow Ti^{4+} + Fe^{2+} \quad (4)$$

$$TiO_2 + h\nu \rightarrow e^- + h^+ \quad (5)$$

$$e^- + O_2 \rightarrow {}^{\bullet}O_2^- \text{ (ROS)} \quad (6)$$

$$h^+ + OH^- \rightarrow {}^{\bullet}OH \text{ (ROS)} \quad (7)$$

$$Fe^{3+} + O^- \rightarrow Fe^{4+} + O_2^- \quad (8)$$

$$Fe^{4+} + OH^- \rightarrow Fe^{3+} + {}^{\bullet}OH \text{ (ROS)} \quad (9)$$

$$Fe^{2+} + O_2 \rightarrow Fe^{3+} + {}^{\bullet}O_2^- \text{ (ROS)} \quad (10)$$

$$\text{ROS} + \text{organic compounds} \rightarrow CO_2 + H_2O \quad (11)$$

To further verify the excellent antifungal activity of $FeTiO_2B$ caused by visible light, the original bamboo and $FeTiO_2B$ were placed in a natural environment without any light. Fig. 11 shows the mould fungi growth on the surfaces of original bamboo and $FeTiO_2B$ after being cultured in the dark environment conditions for one week. As shown in Fig. 11, the original bamboo and the $FeTiO_2B$ were both infected with mould fungi on the surfaces. Without light illumination, the mould fungi grown on $FeTiO_2B$ surfaces, indicating that Fe-doped TiO_2 nanoparticles were not toxic to the mould fungi by themselves. The above results demonstrated that Fe-doped TiO_2 is crucial for inhibition growth of mould fungi on the surface of bamboo under solar light, which can be more effective in the protection and maintenance of bamboo surfaces than pure TiO_2, thus reducing the biodeterioration processes.

4. Conclusions

In summary, visible-light-mediated antifungal bamboo based on Fe-doped TiO_2 thin films was successfully fabricated *via* a facile one-step homogeneous precipitation method. Fe doping exhibits a significant influence on the crystallinity, crystallite size, and photocatalytic activity of the TiO_2 products. Fe doped in the TiO_2 lattice also shifted the optical absorption edge to the visible region. Compared with TiO_2/bamboo, the Fe-doped TiO_2/bamboo exhibited much higher photocatalytic disinfection activity to mould fungi under natural environment. Fe dopants increased the electron–hole pair separation efficiency, inhibited their recombination leading to a lifetime increase of the generated electrons, and thus improved antifungal activity even under nature light. Therefore, Fe-doped TiO_2 photocatalyst has a great potential as an environmentally-friendly alternative method to inhibit mould fungi under solar irradiation for protecting bamboo products.

Conflicts of interest

There are no conflicts to declare.

Acknowledgements

The work was financially supported by the Fundamental Research Funds for the Central Non-profit Research Institution of CAF (CAFYBB2017MA023) and Key Laboratory of High Efficient Processing of Bamboo of Zhejiang Province (2014F10047).

References

1 F. N. Chen, X. D. Yang and Q. Wu, *Environ. Sci. Technol.*, 2009, **43**, 4606–4611.
2 W. Wang, G. Li, D. Xia, T. An, H. Zhao and P. K. Wong, *Environ. Sci.: Nano*, 2017, **4**, 782–799.
3 J. Meng, P. Zhang, F. Zhang, H. Liu, J. Fan, X. Liu, G. Yang, L. Jiang and S. Wang, *ACS Nano*, 2015, **9**, 9284–9291.
4 T. Leshuk, R. Parviz, P. Everett, H. Krishnakumar, R. A. Varin and F. Gu, *ACS Appl. Mater. Interfaces*, 2013, **5**, 1892–1895.
5 I. G. Yu, J. K. Yong, H. J. Kim, C. Lee and I. L. Wan, *J. Mater. Chem.*, 2010, **21**, 532–538.
6 H. Bodaghi, Y. Mostofi, A. Oromiehie, Z. Zamani, B. Ghanbarzadeh, C. Costa, A. Conte and M. A. D. Nobile, *LWT–Food Sci. Technol.*, 2013, **50**, 702–706.
7 T. Matsunaga, R. Tomoda, T. Nakajima and H. Wake, *FEMS Microbiol. Lett.*, 1985, **29**, 211–214.
8 R. Nakano, H. Ishiguro, Y. Yao, J. Kajioka, A. Fujishima, K. Sunada, M. Minoshima, K. Hashimoto and Y. Kubota, *Photochem. Photobiol. Sci.*, 2012, **11**, 1293–1298.
9 L. Rizzo, *J. Hazard. Mater.*, 2009, **165**, 48–51.
10 F. Chen, X. Yang and Q. Wu, *Build. Environ.*, 2009, **44**, 1088–1093.
11 C. A. Linkous, G. J. Carter, D. B. Locuson, A. J. Ouellette, D. K. Slattery and L. A. Smitha, *Environ. Sci. Technol.*, 2000, **34**, 4754–4758.
12 J. Lonnen, S. Kilvington, S. C. Kehoe, F. Altouati and K. G. Mcguigan, *Water Res.*, 2005, **39**, 877–883.
13 J. Zhang, Y. Liu, Q. Li, X. Zhang and J. K. Shang, *ACS Appl. Mater. Interfaces*, 2013, **5**, 10953–10959.

14 A. Flynn, K. W. Chan, Z. H. Zhu and L. Yu, *J. Rural Stud.*, 2017, **49**, 128–139.
15 H. Chi, T. Nguyen, D. Stanley, A. Persily and R. L. Corsi, *Build. Environ.*, 2014, **81**, 226–233.
16 N. C. Birben, C. S. Uyguner-Demirel, S. S. Kavurmaci, Y. Y. Gürkan, N. Turkten, Z. Cinar and M. Bekbolet, *Catal. Today*, 2017, **281**, 78–84.
17 E. Bae, W. Choi, J. Park, H. S. Shin, S. B. Kim and J. S. Lee, *J. Phys. Chem. B*, 2014, **108**, 14093–14101.
18 Z. Zhao, W. Zhang, X. Lv, Y. Sun, F. Dong and Y. Zhang, *Environ. Sci.: Nano*, 2016, **3**, 1306–1317.
19 L. Wang, J. Fan, Z. Cao, Y. Zheng, Z. Yao, G. Shao and J. Hu, *Chem.–Asian J.*, 2014, **9**, 1904–1912.
20 M. Zhou, J. Yu and B. Cheng, *J. Hazard. Mater.*, 2006, **137**, 1838–1847.
21 J. Choi, H. Park and M. R. Hoffmann, *J. Phys. Chem. C*, 2010, **114**, 783–792.
22 A. J. Fonseca, F. Pina, M. F. Macedo, N. Leal, A. Romanowska-Deskins, L. Laiz, A. Gomez-Bolea and C. Saiz-Jimenez, *Int. Biodeterior. Biodegrad.*, 2010, **64**, 388–396.
23 J. Li, J. Xu, W. L. Dai, H. Li and K. Fan, *Appl. Catal., B*, 2009, **85**, 162–170.
24 J. C. Yu, W. Ho, J. Lin, H. Yip and P. K. Wong, *Environ. Sci. Technol.*, 2003, **37**, 2296–2301.
25 W. Zhang, Y. Chen, S. Yu, S. Chen and Y. Yin, *Thin Solid Films*, 2008, **516**, 4690–4694.
26 M. F. L. Russa, A. Macchia, S. A. Ruffolo, F. D. Leo, M. Barberio, P. Barone, G. M. Crisci and C. Urzì, *Int. Biodeterior. Biodegrad.*, 2014, **96**, 87–96.
27 C. C. Trapalis, P. Keivanidis, G. Kordas, M. Zaharescu, M. Crisan, A. Szatvanyi and M. Gartner, *Thin Solid Films*, 2003, **433**, 186–190.
28 EN927-3 Paints and varnishes, *Coating Materials and Coating Systems for Exterior Wood – Part 3 Natural Weathering Test*, European Committee for Standardization, 2000.
29 F. Sun, B. Bao, L. Ma, A. Chen and X. Duan, *J. Wood Sci.*, 2012, **58**, 51–56.
30 J. Lin, Y. Lin, P. Liu, M. J. Meziani, L. F. Allard and Y. Sun, *J. Am. Chem. Soc.*, 2002, **124**, 11514–11518.
31 Y. Niu, M. Xing, J. Zhang and B. Tian, *Catal. Today*, 2013, **201**, 159–166.
32 M. Xing, Y. Wu, J. Zhang and F. Chen, *Nanoscale*, 2010, **2**, 1233–1239.
33 M. Zhou and J. Yu, *J. Hazard. Mater.*, 2008, **152**, 1229–1236.
34 S. Liu, X. Sun, J. G. Li, X. Li, Z. Xiu, H. Yang and X. Xue, *Langmuir*, 2010, **26**, 4546–4553.
35 H. Song, Y. Li, Z. Lou, M. Xiao, L. Hu, Z. Ye and L. Zhu, *Appl. Catal., B*, 2015, **166–167**, 112–120.
36 M. Arienzo, R. Scotti, L. Wahba, C. Battocchio, E. Bemporad, A. Nale and F. Morazzoni, *Appl. Catal., B*, 2009, **93**, 149–155.
37 J. Ng, S. Xu, X. Zhang, Y. Y. Hui and D. D. Sun, *Adv. Funct. Mater.*, 2011, **20**, 4287–4294.
38 H. Yu, H. Irie, Y. Shimodaira, Y. Hosogi, Y. Kuroda, M. Miyauchi and K. Hashimoto, *J. Phys. Chem. C*, 2010, **114**, 16481–16487.
39 J. Li, H. Yu, Z. Wu, J. Wang, S. He, J. Ji, N. Li, Y. Bao, C. Huang and Z. Chen, *Colloids Surf., A*, 2016, **508**, 117–123.
40 T. Tong, J. Zhang, B. Tian, F. Chen and D. He, *J. Hazard. Mater.*, 2008, **155**, 572–579.
41 C. Sichel, M. D. Cara, J. Tello, J. Blanco and P. Fernández-Ibáñez, *Appl. Catal., B*, 2007, **74**, 152–160.

